VU Research Portal

A combined diffusion-weighted and electroencephalography study on age-related differences in connectivity in the motor network during bimanual performance

Babaeeghazvini, Parinaz; Rueda-Delgado, Laura Milena; Zivari Adab, Hamed; Gooijers, Jolien; Swinnen, Stephan; Daffertshofer, Andreas

document version
Publisher's PDF, also known as Version of record

document license
Article 25fa Dutch Copyright Act

Link to publication in VU Research Portal

WILEY

RESEARCH ARTICLE

A combined diffusion-weighted and electroencephalography study on age-related differences in connectivity in the motor network during bimanual performance

Parinaz Babaeeghazvini[1] | Laura Milena Rueda-Delgado[2] | Hamed Zivari Adab[2] | Jolien Gooijers[2] | Stephan Swinnen[2,3] | Andreas Daffertshofer[1]

[1]Amsterdam Movement Science Institute (AMS) and Institute for Brain and Behaviour Amsterdam (iBBA), Faculty of Behavioural and Movement Sciences, Vrije Universiteit, Amsterdam, The Netherlands

[2]Department of Movement Sciences, Movement Control and Neuroplasticity Research Group, KU Leuven, Leuven, Belgium

[3]Leuven Brain Institute (LBI), Leuven, Belgium

Correspondence
A. Daffertshofer, Amsterdam Movement Science Institute (AMS) and Institute for Brain and Behaviour Amsterdam (iBBA), Faculty of Behavioural and Movement Sciences, Vrije Universiteit, van der Boechorststraat 9, 1081 BT Amsterdam, The Netherlands.
Email: a.daffertshofer@vu.nl

Abstract

We studied the relationship between age-related differences in inter- and intra-hemispheric structural and functional connectivity in the bilateral motor network. Our focus was on the correlation between connectivity and declined motor performance in older adults. Structural and functional connectivity were estimated using diffusion weighted imaging and resting-state electro-encephalography, respectively. A total of 48 young and older healthy participants were measured. In addition, motor performances were assessed using bimanual coordination tasks. To pre-select regions-of-interest (ROIs), a neural model was adopted that accounts for intra-hemispheric functional connectivity between dorsal premotor area (PMd) and primary motor cortex (M1) and inter-hemispheric connections between left and right M1 ($M1_L$ and $M1_R$). Functional connectivity was determined via the weighted phase-lag index (wPLI) in the source-reconstructed beta activity during rest. We quantified structural connectivity using kurtosis anisotropy (KA) values of tracts derived from diffusion tensor-based fiber tractography between the aforementioned areas. In the group of older adults, wPLI values between $M1_L$–$M1_R$ were negatively associated with the quality of bimanual motor performance. The additional association between wPLI values of PMd_L––$M1_L$ and PMd_R–$M1_L$ supports that functional connectivity with the left hemisphere mediated (bimanual) motor control in older adults. The correlational analysis between the selected structural and functional connections revealed a strong association between wPLI values in the left intra-hemispheric PMd_L–$M1_L$ pathway and KA values in $M1_L$–$M1_R$ and PMd_R–$M1_L$ pathways in the group of older adults. This suggests that weaker structural connections in older adults correlate with stronger functional connectivity and, hence, poorer motor performance.

KEYWORDS

aging, bimanual coordination, DWI, EEG, functional connectivity, motor control, structural connectivity

1 | INTRODUCTION

Bimanual coordination requires a fine-tuned interaction between limbs and muscles. Aging may jeopardize this interaction potentially yielding a decline in bimanual performance with potential impact on daily life activities. The decline can vary as aging may affect various levels of the motor system, from muscle to cortical atrophy. White

matter structural connectivity in the brain alters at large scale while being most pronounced in inter-hemispheric connections (Abe et al., 2002; Nusbaum, Tang, Buchsbaum, Wei, & Atlas, 2001; O'Sullivan et al., 2004; Sullivan et al., 2001). Hence, it does not come as a surprise that correlations between age-related structural differences in the brain and bimanual performance have already been demonstrated. Serbruyns et al. (2015) reported significant associations between

deteriorated bimanual motor performance and altered structural organization of inter-hemispheric pathways, assessed via fractional anisotropy (FA) values of the corpus callosum (CC). Fujiyama, Van Soom, Rens, Gooijers, et al. (2016) found that the white matter (WM) microstructural organization of inter-hemispheric fiber tracts between nonprimary and primary motor regions (left dorsal premotor, PMd, to right M1) correlated significantly with the quality of bimanual coordination in older adults when the left hand had to move faster than right hand. PMd appears also involved in the selection of an action under particular task conditions (Boussaoud & Wise, 1993; Crammond & Kalaska, 1994; Di Pellegrino & Wise, 1993; Shen & Alexander, 1997; Wise, Di Pellegrino, & Boussaoud, 1992).

Other studies also demonstrated correlations between age-related differences in functional connectivity and bimanual performance. Using bilateral paired-pulse transcranial magnetic stimulation (TMS), Hinder, Fujiyama, and Summers (2012) identified a pronounced reliance on inter-hemispheric functional connectivity between PMd and contralateral M1 in older adults during performance of a bimanual sensorimotor reaction time task. Solesio-Jofre et al. (2014) reported correlations between age-related increases in resting state functional connectivity of inter-hemispheric dorsal and ventral premotor areas and diminished bimanual performance.

Connections between homologous bilateral motor areas are known to cause cross talk between hemispheres. When excitatory, this cross talk may be manifested in the occurrence of mirror movements, that is, associated movements in limbs that are not intended to move (Armatas, Summers, & Bradshaw, 1994; Daffertshofer, van den Berg, & Beek, 1999; Gerloff, Corwell, Chen, Hallett, & Cohen, 1998; Leinsinger et al., 1997). Zooming into this cross talk indicated that a loss of M1 inhibition through PMd in the same hemisphere can result in movement instabilities (Daffertshofer, Peper, & Beek, 2005). That is, intra-hemispheric inhibition may help to prevent the co-activation of cortical muscle representations, thus enhancing motor contrast and the selectivity of muscle activation during the performance of (a)symmetric bimanual tasks (Stinear & Byblow, 2002). To what extent the delicate balance between functional inter-hemispheric and intra-hemispheric interactions are jeopardized by age-related structural changes in the brain is yet unknown.

In the motor system structural and functional connectivity are closely associated. Wahl et al. (2007) demonstrated a positive correlation between FA of M1-M1 callosal motor fibers and the interhemispheric inhibition in healthy young individuals. Fujiyama, Van Soom, Rens, Gooijers, et al. (2016) extended this for older adults and to non-homologous interhemispheric connections. Several fMRI studies indicated the higher activity of dorso-lateral pre-frontal cortex (DLPFC) and PMd in older adults during the performance of inter-limb (Heuninckx, Wenderoth, Debaere, Peeters, & Swinnen, 2005; Heuninckx, Wenderoth, & Swinnen, 2008) and bimanual coordination tasks (Goble et al., 2010). Fujiyama, Van Soom, Rens, Gooijers, et al. (2016) determined FA values for pairwise inter-hemispheric interactions between (pre)motor regions, including bilateral M1, PMd and DLPFC, and related them to the degree of modulation of inter-hemispheric functional interactions during bimanual coordination tasks using a dual-site TMS paradigm incorporating paired-pulse TMS to examine the time course of interactions in a "two-node" neural circuit with two different coils. Modulatory capability of inter-hemispheric interactions between PMd and contralateral M1 turned out to be intact in older as compared with young adults whereas the interaction between DLPFC and M1 seemingly changed as a function of age, possibly accounting for impaired motor performance. However, the detailed relation between (age-related differences in) structural connectivity and functional connectivity in both intra- and inter-hemispheric connections between PMd and M1 and their association with bilateral M1 connection remained unclear.

To unravel the association between age-related structural differences in inter- and intra-hemispheric connections ($M1_L$–$M1_R$ and PMd–M1) and the functional interplay between them, we adopted a bimanual coordination task and used diffusion weighted imaging (DWI) to estimate structural connectivity and resting state electroencephalography (EEG) as proxy of functional connectivity. In light of the expected roles of inter-hemispheric excitation versus intra-hemispheric inhibition in such coordination tasks (cf. Daffertshofer et al., 2005), we particularly focused on M1-M1 and PMd-M1 structural and functional pathways. To explicitly address differences in structure and function, we compared a group of younger and older participants. We expected poorer motor performance and reduced structural connectivity in the group of older adults and hypothesized this to be accompanied by age-related differences in inter- and intra-hemispheric functional connectivity, in line with the aforementioned model.

2 | MATERIALS AND METHODS

2.1 | Participants

Two groups of healthy adults participated in the study: 24 young (10 male; mean age 26 years; range 21–32 years) and 24 older adults (17 male; mean age 67 years; range 60–74 years). DWI data were not acquired for two elderly and two young subjects. DWI data of one subject from each group were excluded from analysis due to excessive head motion. All participants were right-handed according to the Oldfield Handedness Questionnaire (Oldfield, 1971), except for one older participant. Oldfield scores were: mean 91.4, range 53–100 for the young and mean 92.6, range 24–100 for the older participants. Older adults were also assessed with the Montreal Cognitive Assessment (MOCA) test (Nasreddine et al., 2005). The MOCA cut-off of 25 excluded four older participants from further analysis. Data from 21 younger (9 male) and 17 older adults (12 male) entered subsequent analyses. Participants self-reported their neurological and psychiatric status. MRI scans were evaluated for both abnormalities and acquisition artifacts. The experiment was approved by the local Ethics Committee of K.U. Leuven and was performed in accordance with the 1964 Declaration of Helsinki. All the participants signed an informed consent form prior to experimental assessments.

2.2 | Procedures

Participants practiced a bimanual visuomotor task based on a one previously used in our laboratory (Chalavi et al., 2016; Gooijers et al.,

2013; Rueda-Delgado et al., 2017; Zivari Adab et al., 2018). Participants were asked to rotate two shafts (left/right), mounted on rotating disks, with their hands while the forearms rested over ramps, which were placed on a desk. Participants could not see their hands/forearms as a wooden frame was placed over their hands/forearms. The data from the angular encoders were recorded and online processed with LabView 8.5 (National Instruments, Austin, Texas, USA).

Cyclical rotation of the shafts caused a white cursor (visual feedback) to move on the computer screen in front of the participant. The task was to make sure the cursor followed an inclined blue line (presented on the screen) with a predefined speed. Clockwise and counter-clockwise rotation of the right dial moved the cursor from the center to the right upper and left lower quadrant, respectively. Movement of the cursor to the left upper and right lower quadrant happened via counter-clockwise and clockwise rotation of the left dial, respectively. Rotation of both dials hence moved the cursor on the inclined line. The slope of that line prescribed the required coordination between left and right movements. We employed three tasks: (1) iso-frequency movements (1:1 frequency ratio) with a target line along the vertical axis, (2) a polyrhythm (2:5 frequency ratio) for which the right hand moved faster (the target line pointed right with a slope of 68.2°), and (3) a mirrored polyrhythm (5:2 frequency ratio) with the left hand moving faster (target line pointed left with a slope 111.8° from midline). Participants were instructed to match the red cursor with the target line as accurately as possible for 8 s (the duration of a full line according to the predefined speed, see Figure 1).

Participants were familiarized with the task by practicing unimanual movements (resulting in straight lines with 45° to the right for the right-hand movement and 135° to the left for the left-hand movement). During this familiarization, the resulting red line drawn from the unimanual movement was visible during movement along with the cue line (online visual feedback). A temporal cue was provided in the form of a white dot moving along the target line. In this familiarization,

participants needed to follow the tempo of the white target. Subsequently, a baseline recording was conducted whereby the bimanual task was conducted without visual feedback. Subjects performed three blocks of 15 lines each (5 trials per task). The presentation of these tasks was counter-balanced. The target line was presented for 2 s, after which participants were prompted to initiate movement. This was followed by four training sessions distributed over four non-consecutive days (within 8 days). During these training sessions, visual feedback of performance was provided for 2 s after trial only (~knowledge of performance). During training, subjects performed the task for approximately 30 min in 6 blocks of 15 trials each (30 trials per task). On the last day, following the fourth practice session, a retention test was acquired without after-trial visual feedback similar to the baseline measure.

The results reported in the current article pertain to the behavior, obtained during the test, and resting-state EEG recordings obtained prior to the retention test, in which both young and older adults had reached a stable level of performance.

2.3 | Data acquisition

2.3.1 | Motor behavior

The rotating discs contained incremental rotary encoders for registration of angular displacement (ICURO RI32 Hengstler, Aldingen, Germany, accuracy $\Delta\alpha$ = 0.0879° given one pulse over 4,096 pulses per revolution, sample frequency 250 Hz); see, for example, (Gooijers et al., 2013; Rueda-Delgado et al., 2017; Serbruyns et al., 2015; Sisti et al., 2011) for previous applications.

2.3.2 | MRI/DWI

A Philips Ingenia 3 T CX MRI scanner with standard head coil served for image acquisition. First, a high-resolution T1-weighted structural image was acquired using a 3D-turbo field echo (3DTFE) sequence for
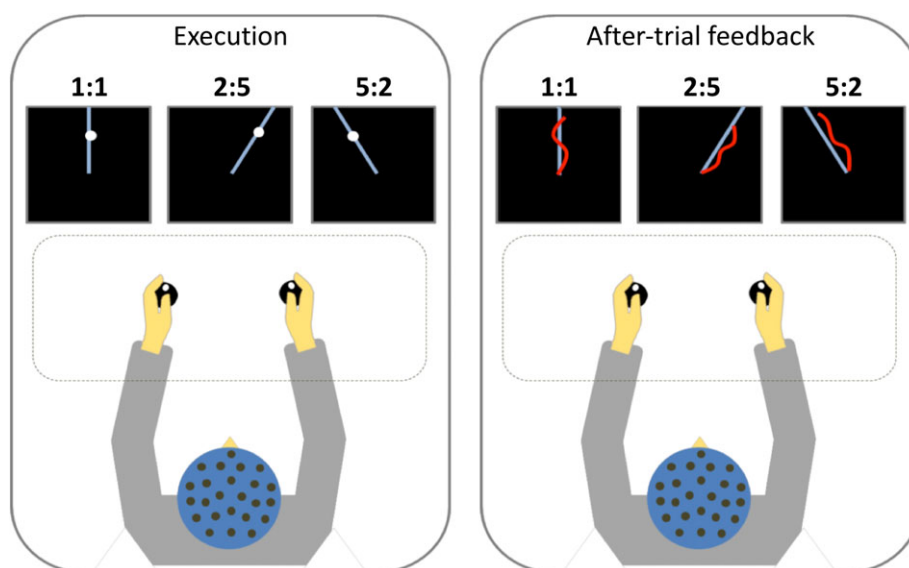
FIGURE 1 Illustration of the motor task. Participants were asked to rotate two disks (left/right) to move a cursor visible after execution of the movement. A particular ratio of rotational frequency yielded movement along a prescribed line. The direction of the line discriminated three different frequency ratios. During execution of the tasks (8 s) no online feedback was provided (left panel). After every trial, feedback of the performance was displayed as shown for 2 s (right panel) [Color figure can be viewed at wileyonlinelibrary.com]
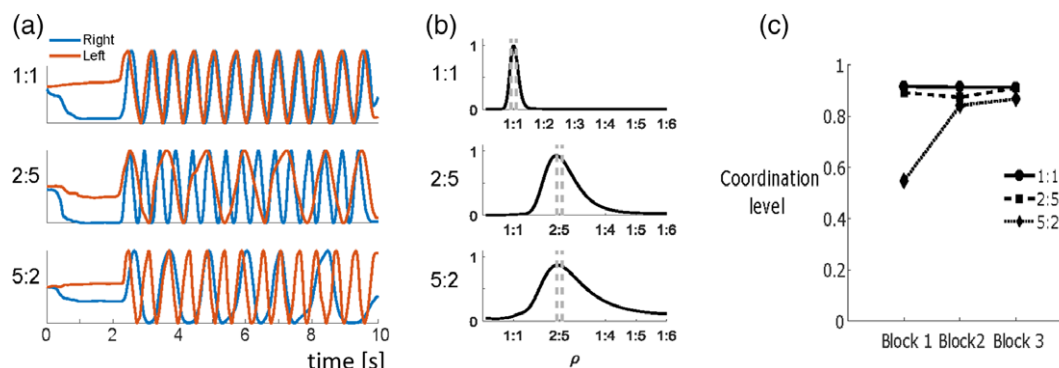
FIGURE 2 The panels illustrate the bimanual performance in three tasks with 1:1, 2:5, and 5:2 ratios. (a) Radial trajectories of wrist rotations. (b) Cross-spectral overlap Ψ of trials across different *p*-values. Dashed lines indicate the window of target ratio. The average value in this window served as a measure of performance. (c) Averaged measures of performance across five trials per task creating one block in one young participant. Participants executed the task in three blocks. Data are from the retention test [Color figure can be viewed at wileyonlinelibrary.com]

anatomical detail (182 contiguous coronal slices, field of view (FOV) = 250 × 250 mm^2, time echo (TE) = 4.6 ms, time repetition (TR) = 9.7 ms, time inversion = 1,000 ms, slice thickness = 1.2 mm, in plane resolution = 0.98 × 0.98 mm^2). Multi-shell high angular resolution diffusion imaging (HARDI) was acquired as follows: single shot spin-echo; TR = 11,000 ms, TE = 82 ms, matrix size of 96×96 and 50 axial slices, voxel size of 2.5 × 2.5 × 2.5 mm^3. Diffusion weightings of 1,000, 2,000, and 3,000 s/mm^2 were applied along 17, 30, and 50 uniformly distributed directions, respectively. In addition, six images without diffusion weighting were obtained at the beginning of the acquisition, immediately preceding the weighted images. Thus, weighted and nonweighted diffusion images were acquired closely in time.

2.3.3 | EEG

We used a 128-channel amplifier (ANT, Enschede, Netherlands, Ag/AgCl electrodes) to record the EEG in a 10/5 montage with common reference. Two bipolar electrodes served to record the electrooculography (EOG). Two additional bipolar electrodes were attached above the left and right flexor carpi radialis to measure the corresponding surface electromyography (EMG). Signals were sampled at a rate of 1,024 Hz. Electrode positions were estimated using an infrared Polaris Spectra camera (NDI, Ontario, Canada) digitized using Neuro-Navigation Visor 2 XT system (ANT). Resting-state activity was recorded at the beginning of each experimental session before the behavioral tasks. Participants had to gaze at a white cross for 3 min and were asked to relax and not to focus their attention on anything particular.

2.4 | Data analysis

2.4.1 | Motor behavior

We estimated the power spectral densities of the signals *x* and *y* of hand rotation using Welch's periodogram method (4 s Hanning windows with 50% overlap). With these estimates we determined the quality of bimanual performance for every trial and every task using the spectral overlap Ψ_x^y (Daffertshofer, Peper, Frank, & Beek, 2000; Houweling, Beek, & Daffertshofer, 2010). That measure quantifies the

level of frequency synchronization between two signals *x* and *y* at a given ratio *ρ*. It is defined as:

$$\Psi_x^y(\rho) = \frac{2 \int P_x(f)P_y(\rho f)df}{\int \left[P_x{}^2(f) + P_y{}^2(\rho f)\right]df}$$

where, P_x and P_y are the power spectral densities of the dials' rotation. As said, *ρ* represents the frequency ratio of movement in the different experimental tasks (*ρ* = 1 for iso-frequency movement 1:1, *ρ* = 2.5 for polyrhythm 2:5, and *ρ* = 2.5 for the mirrored polyrhythm 5:2 with the inverted signals). $\Psi_x^y(\rho)$ values are ranged from 0 to 1 with 1 indicating the best bimanual performance. This analysis was performed in Matlab (Mathworks, MA, version R2015b). Figure 2 shows three examples of the shape of the function $\Psi_x^y(\rho)$.

2.4.2 | MRI/DWI

DWIs were pre-processed and analyzed in ExploreDTI (version 4.8.6) (Leemans, Jeurissen, Sijbers, & Jones, 2009). Every DWI volume was evaluated for artifacts (large signal dropouts) by visual inspection. Visual inspection was performed in different orthogonal views of each image to check for inter-slice and intra-volume instabilities ("zebra patterns" or "zipper" artifact) (Tournier, Mori, & Leemans, 2011). Further potential artifacts were identified via the residual map, revealing the difference between the modeled and the measured signal (Tournier et al., 2011). After visual inspection and removing volumes with artifacts (one volume for six subjects; two older adults; and four younger adults), the DWI data sets were corrected in one interpolation step for motion, eddy current, and EPI susceptibility distortions (Irfanoglu, Walker, Sarlls, Marenco, and Pierpaoli (2012). The EPI susceptibility distortions were corrected by registering the DWI images to undistorted T1 images (Leemans, Sijbers, De Backer, Vandervliet, & Parizel, 2005; Van Hecke et al., 2007). The B-matrix was reoriented accordingly. A robust extraction of kurtosis indices with linear estimation (REKINDLE) was applied to estimate the DTI/DKI metrics from the entire diffusion data set (Tax, Otte, Viergever, Dijkhuizen, & Leemans, 2015).

For every subject, whole brain deterministic streamline tractography was performed to reconstruct white matter tracts (Basser, Pajevic, Pierpaoli, Duda, & Aldroubi, 2000). Tractography parameters were set
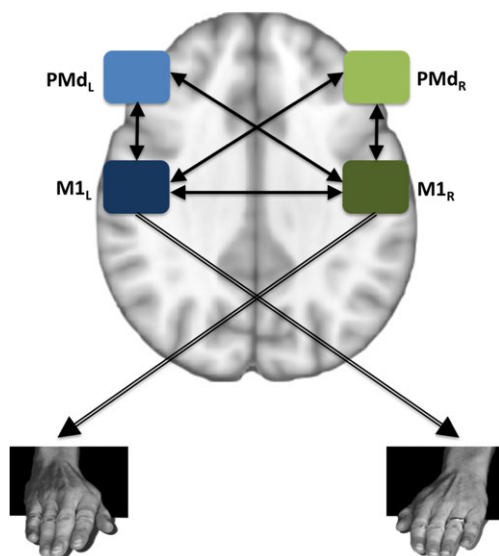
FIGURE 3 The selected regions-of-interest (ROIs) and their connections according to the model of functional connectivity by Daffertshofer et al. (2005) [Color figure can be viewed at wileyonlinelibrary.com]

as follows: seed point resolution of $2 \times 2 \times 2$ mm^3; seed FA threshold of 0.15 (FA tracking threshold range from 0.15 to 1), fiber length-range from 10 to 500 mm, angle threshold of 30° and step size of 2 mm.

Left/right M1 ($M1_L$/$M1_R$) and left/right PMd (PMd_L/PMd_R) were selected as regions of interest (ROIs) for connectivity analysis. We used the Human Motor Area Template (HMAT) (http://lrnlab.org/) (Mayka, Corcos, Leurgans, & Vaillancourt, 2006) to extract these ROIs. ROIs were transformed into native space (T1-weighted space) by using the inverse warp of the nonlinear registration from T1 to MNI space. Visual inspection of each subject's DWI data and the extracted ROIs served to confirm proper transformation of DWI images and correct positioning of the ROIs.

We considered only the fibers passing through both ROIs as listed in pairs: $M1_L$–$M1_R$, PMd_L–$M1_R$, PMd_R–$M1_L$, PMd_R–$M1_R$, and PMd_L–$M1_L$; see Figure 3.

Connectivity values between two ROIs were calculated by (i) averaging KA values (Poot, den Dekker, Achten, Verhoye, & Sijbers, 2010) along the streamlines $ROI_1 \rightarrow ROI_2$; (ii) estimating inter-quartile range (IQR) values from the obtained mean KA values (i.e., values were ordered and then divided into four equal parts); (iii) selecting the first quartile value (IQR_L; median value of the lower half of data) for further analysis as it turned out to have the maximum discriminative power; (iv) repeating (i, ii, and iii) for the streamlines $ROI_2 \rightarrow ROI_1$; (v) computing mean values between obtained IQR_L KA values of $ROI_1 \rightarrow ROI_2$ and $ROI_2 \rightarrow ROI_1$; we note that left/right differences were minor allowing for using their averaged value. Figure 4 illustrates the results of the tractography using two seminal examples.

For the sake of completeness, we also repeated these steps for the fractional anisotropy (FA) mean diffusivity (MD), radial diffusivity (RD), and axial diffusivity (AD); the corresponding results can be found in the Appendix (Table A6).

2.4.3 | EEG

EEG recordings of the resting state were band-pass filtered at 1–100 Hz, and notch-filtered at 50 Hz. To minimize artifacts, three steps were taken following Rueda-Delgado et al. (2017). First, epochs were redefined as 2-s segments and channels with voltage levels exceeding 150 μV were rejected. Second, eye blinks and movement artifacts were extracted form EEG signals through independent component analysis (ICA). Components with the largest weights of the mixing matrix contributing to EOG channels and components related to movement artifacts based on their spectral properties, and their spatial and temporal kurtosis were selected to be removed (Nolan, Whelan, & Reilly, 2010). Third, the z-score was estimated for large kurtosis and large spectral power (with frequencies over 50 Hz) in each epoch, and epochs with z-score value larger than 3 were rejected. These analyses were performed in Matlab (Mathworks, MA, version R2015b) involving the open-source Fieldtrip toolbox (Oostenveld, Fries, Maris, & Schoffelen, 2011).

A 6-tissue finite element model was applied to estimate subject-specific head models based on their T1-weighted images using the Fieldtrip-SIMBIO integration toolbox (Buchner et al., 1997). Tissues included skin, compact bone, spongy bone, cerebro-spinal fluid (CSF), cortical and cerebellar gray matter, and cortical and cerebellar white matter. Following Iacono et al. (2015) normalization was realized by warping a high-resolution template of the human head and neck using SPM12 (www.fil.ion.ucl.ac.uk/spm/software/spm12; see also www.itis.ethz.ch/virtual-population/regional-human-models/mida-model/mida-v1-0). Skin, compact bone, spongy bone, CSF, gray, and white matter compartments were given conductivity values of 0.2, 0.0063, 0.04, 1.5385, 0.333, and 0.1429 S/m, respectively (Holdefer, Sadleir, & Russell, 2006; Wagner et al., 2014; Wolters et al., 2006).

Iterative closest point algorithm was applied to align the electrode positions on the skin. To find the locations of possible sources on the cortical and cerebellar gray matter, the segmented brain volume was divided in a regular 3D grid with 5-mm resolution. The lead field was estimated based on the participant's head model, the electrode positions, and the 3D grid.

The covariances between all electrodes along with the lead field matrix were used to determine linearly-constrained minimum variance beamformer (Van Veen, van Drongelen, Yuchtman, & Suzuki, 1997). The beamformer served to reconstruct the single-trial time series as a virtual channel at the voxel level within the beta frequency band (15–30 Hz); we used the dominant component from a singular-value decomposition of the 3D-projected virtual channel as time series (Darvas, Pantazis, Kucukaltun-Yildirim, & Leahy, 2004). The beamformers were estimated in four regions of the HMAT atlas: $M1_L$/$M1_R$ and PMd_L/PMd_R, in agreement with ROIs used in the assessment of structural connectivity (see above).

Functional connectivity between the pairs of the source-localized regions $M1_R$–$M1_L$, PMd_L–$M1_L$, PMd_L–$M1_R$, PMd_R–$M1_L$, and PMd_R–$M1_R$ were determined via the weighted phase-lag index (wPLI) (Hardmeier et al., 2014; Vinck, Oostenveld, van Wingerden, Battaglia, & Pennartz, 2011). The wPLI is a modification of the PLI (Stam, Nolte, & Daffertshofer, 2007) which estimates the leading or lagging node in a pair of signals by weighting each phase difference with the
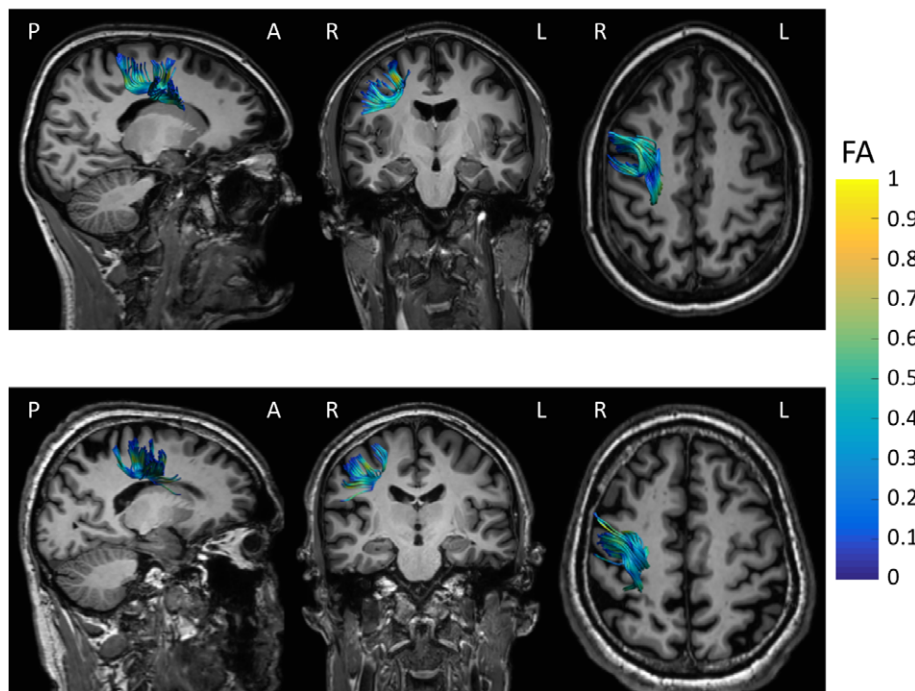
FIGURE 4 Two examples of the extracted tracts between PMd_R and $M1_R$. Upper row: A younger participant, lower row: An older participant. The tracts are displayed on the participant's T1 image. Colors represent FA values, ranged from 0 to 1; A: Anterior, P: Posterior, R: Right, L: Left [Color figure can be viewed at wileyonlinelibrary.com]

imaginary part of the cross-spectra as a factor. This weighting factor makes the wPLI robust to confounding effects of volume conduction (Nolte et al., 2004), It is computed from the cross-spectral density C_{xy} between two virtual sensor time-series in the beta frequency band (15–30 Hz) by means of

$$wPLI = \frac{|\langle |\Im(C_{xy})| \, sign((\Im(C_{xy})))\rangle|}{\langle |\Im(C_{xy})|\rangle}$$

where, $|\cdots|$ denotes for modulus, $\langle\cdots\rangle$ the average value (as a proxy of the expectation value) and $\Im(\cdots)$ imaginary part of the cross-spectral density C_{xy}; $sign(\cdots)$ refers to the signum function. The wPLI values generally range between 0 and 1. No coupling between time series yields a symmetric, uniform phase distribution and, thus, results in a wPLI value near or equal to zero. On the other hand, a consistent phase-locking between two time-series implies a unimodal distribution of phase differences resulting in a wPLI value larger than zero (smaller or equal to one) whenever that distribution is not centered around zero or $\pm\pi$; the latter cases may be caused by volume conduction while a distribution off-centered these isolated points indicates "true" interactions between sources.

3 | STATISTICS

We aimed for investigating age-related differences in bimanual performance, structural and functional connectivity. We hence analyzed the retention test where the age-related difference in bimanual performance was arguably most evident.

We employed three linear mixed effect (LME) models (Pinheiro & Bates, 2000). Model 1: Ψ addressed the behavioral

frequency locking (for average of trials per task), model 2: KA addressed the white matter structural connectivity, and model 3: wPLI addressed the functional connectivity for its associations with age (younger and older adults), behavioral task (1:1, 2:5, and 5:2 coordination), and pathway ($M1_L$–$M1_R$, PMd_L–$M1_L$, PMd_R–$M1_R$, PMd_R–$M1_L$, and PMd_L–$M1_R$). We used the maximum likelihood to estimate the variance of the factor "participant ID" that was entered as a random effect to account for between individual dependence. In model 1, we assessed two fixed effects of age and task as independent variables and their interaction:

$$\Psi_{ij} = (\beta_0 + d_{0j}) + \beta_1(age_j) + \beta_2(task_i) + \beta_3(age_j \times task_i) + \varepsilon_{ij}$$

Here d_{0j} represents the random effect of participant ID in group j, $\beta_{0, 1, 2, 3}$ are the fixed effects and ε_{ij} contains residual errors for task i in group j.

Models 2 and 3 served to assess the two fixed effects of age and pathway and their interaction for KA and wPLI as dependent variables. They read

$$KA_{ij} = (\beta_0 + d_{0j}) + \beta_1(age_j) + \beta_2(pathway_i) + \beta_3(age_j \times pathway_i) + \varepsilon_{ij}$$

and

$$wPLI_{ij} = (\beta_0 + d_{0j}) + \beta_1(age_j) + \beta_2(pathway_i) + \beta_3(age_j \times pathway_i) + \varepsilon_{ij}$$

Normality of the residual distributions was verified by normal probability plot (P–P plot) and, subsequently, by a Shapiro–Wilk test. For post-hoc testing we used nonparametric pairwise comparisons (Mann–Whitney test).

Next, to assess possible associations between structural (KA) and functional connectivity (wPLI) of the selected pathways on the one hand and behavioral performance on the other hand, three stepwise

multiple linear regression analyses (for three different tasks) were conducted for each age group separately (without correction for multiple comparison). All the data (Ψ, KA, and wPLI) were tested for outliers prior to entering the models. The spectral overlap in the 1:1 task displayed outliers (values exceeded mean $\pm$ 3 SD over all data): two for the older adults and one for the younger adults; and KA in PMd_L–$M1_R$ one for the older adults. These data were removed. For each model, the spectral overlap (Ψ) entered as a dependent variable, and KA and wPLI of pathways of interest were included as independent variables. The values of F-to-enter and F-to-remove were 0.05 and 0.1, respectively. The resulting standardized regression coefficient β quantified the strength of the association between bimanual task performance and the respective independent variable. Additionally, we estimated Spearman rank coefficients to test for correlations between wPLI values and between KA and wPLI without correcting for multiple comparisons.

Statistics was performed in SPSS (IBM SPSS Inc., Chicago, version 24).

4 | RESULTS

Due to the lack of DWI data for some subjects, having failed the MOCA test and one excessive head motion, we were left with a total of 38 subjects (21 younger and 17 older adults) to perform our main analyses.

4.1 | Motor behavior—Frequency locking (Ψ)

The average degree of frequency locking between the two hands is shown in Figure 5.

The LME model revealed significant two-way interactions and significant main effects for age and task on spectral overlap. There was a significant effect of age ($F[1,38]$ = 12.726, p < 0.001); older adults performed worse than younger adults (mean difference of 0.155[0.043], 95% CI [0.067–0.242]). There was also a main effect of task ($F[2,76]$ = 41.923, p < 0.0001), with the 1:1 ratio task showing a better performance compared with the other two noniso-frequency tasks. The mean values for different tasks were: mean $\pm$ SE = 0.901 $\pm$ 0.028 for the 1:1 ratio; 0.643 $\pm$ 0.028 for the 2:5 ratio; and 0.660 $\pm$ 0.028 for the 5:2 ratio. Furthermore we found a significant age×task interaction ($F[2,76]$ = 5.359, p < 0.007); the group of older adults performed significantly worse in the noniso-frequency tasks (2:5, 5:2) than the group of younger adults, while their performance for the 1:1 ratio did not differ significantly from the younger group. More details are listed in Tables A1–A3 in the Appendix.

4.2 | MRI/DWI—Structural connectivity (KA)

IQR_L KA values in the five selected pathways for both age groups are depicted in Figure 6. Model 2 revealed a significant fixed effect of age ($F[1,38]$ = 4.875, p = 0.033); older adults had lower KA values (mean $\pm$ SE = 0.203 $\pm$ 0.006) than younger adults (0.219 $\pm$ 0.005) across all five pathways. There was a significant effect of pathway ($F[4,152]$ = 41.978, p < 0.0001) with higher KA
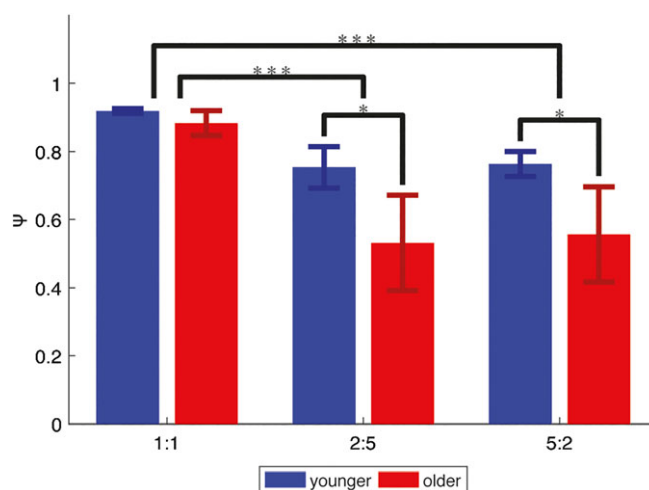

FIGURE 5 Mean level of the spectral overlap Ψ for each movement frequency ratio in young and older adults. Older adults showed worse performance than younger adults across all frequency ratios, that is, behavioral tasks, as reflected by a smaller spectral overlap. However, not all ratios yielded significant differences. Error bars indicate the 95% CI; * indicates significant effects with p < 0.05 and *** p < 0.001 [Color figure can be viewed at wileyonlinelibrary.com]

values for inter-hemispheric connections relative to intra-hemispheric connections. The mean values ($\pm SE$) across age groups were for PMd_R–$M1_R$: 0.185 $\pm$ 0.005, PMd_L–$M1_L$: 0.187 $\pm$ 0.005, PMd_L–$M1_R$: 0.229 $\pm$ 0.005, PMd_R–$M1_L$: 0.234 $\pm$ 0.005, and $M1_L$–$M1_R$: 0.220 $\pm$ 0.005; see Tables A4 and A5 in the Appendix for more detail. The post-hoc Mann Whitney test revealed that only the KA-values of PMd_R–$M1_R$ was significantly decreased in the older adults (p = 0.009); compare Table A6 in the Appendix. We could not establish a significant interaction between age and pathway ($F[4,152]$ = 1.628, p = 0.017).

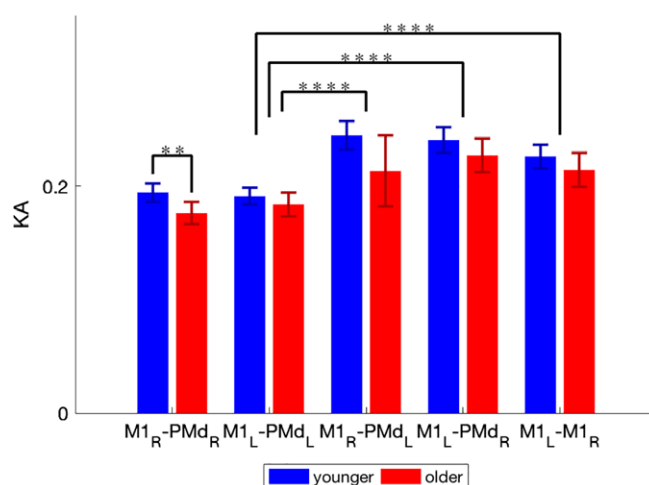**FIGURE 6** KA values in younger and older adults. KA values were significantly lower in older adults than younger adults across all pathways of interest. Post-hoc tests revealed that only the KA-values of PMd_R–$M1_R$ was significantly decreased in the older adults. Error bars indicate the 95% CI; ** indicates significant effects with p < 0.01, **** p < 10^{-4} [Color figure can be viewed at wileyonlinelibrary.com]
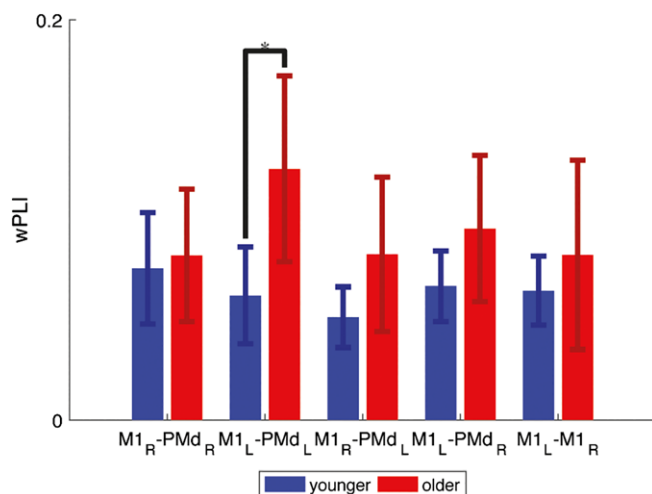
FIGURE 7 Functional connectivity (wPLI) between pairs of cortical regions in young and older adults. The wPLI value of PMd_L–$M1_L$ was significantly increased in older adults. Error bars indicate the 95% CI; * indicates significant effects with $p < 0.05$ [Color figure can be viewed at wileyonlinelibrary.com]

4.3 | EEG—Functional connectivity (wPLI)

We found a significant main effect of age ($F[1,38] = 4.916$, $p = 0.033$), indicating that older adults had higher wPLI values (mean $\pm$ SE = 0.094 $\pm$ 0.010) than younger adults (0.064 $\pm$ 0.009). However, there was no significant main effect of pathway ($F[4,152] = 1.113$, $p = 0.353$) and no significant interaction effect between age and pathway ($F[4,152] = 1.264$, $p = 0.287$). Figure 7 provides an overview of the phase locking index values. The post-hoc assessment revealed that the wPLI value of PMd_L-$M1_L$ was significantly increased in older adults with respect to younger adults ($p = 0.018$). All results are summarized in the Appendix (Tables A7–A9).

4.4 | Association between motor behavior, structural connectivity, and functional connectivity

The stepwise multiple regression revealed that functional and structural connectivity were related to motor performance in both groups.
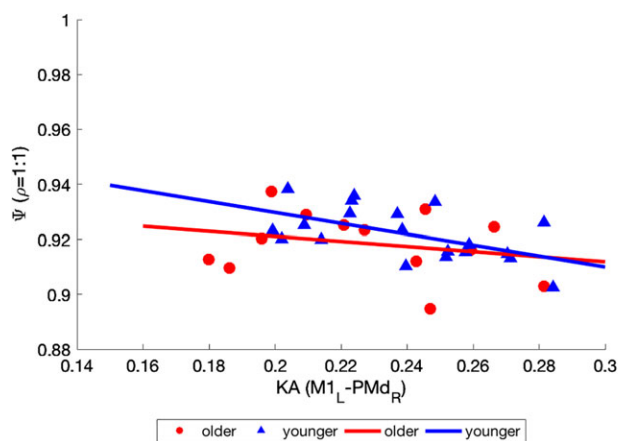
Our results indicated that higher quality of performance in the 1:1 task (i.e., the right hand rotates as fast as the left hand) was significantly associated with lower KA values between PMd_R and $M1_L$ within the young group ($\beta = -0.552$, $p = 0.012$). We also found wPLI values between inter-hemispheric primary motor cortexes ($M1_L$–$M1_R$) to be predictive for bimanual performance in the 5:2 ratio, that is, when the left hand rotates faster than the right hand, (less neural synchronization, i.e., weaker functional coupling). That was true within the older group ($\beta = -0.540$, $p = .031$); see also Figure 8.

We did not find any significant association between motor performance in 2:5 ratio and all KA/wPLI values considered here. The Appendix (Table A10) provides more detail about the outcome of the regression analyses.

4.5 | Correlation between functional connections (wPLI)

We estimated Spearmen rank coefficients to test for correlations between wPLI values of our pathways of interest. Only within the group of older adults, the wPLI value between PMd_R–$M1_L$ correlated positively with the wPLI value of PMd_L–$M1_L$ connection (see Figure 9 and Table A11 in the Appendix for an overview). Since our multiple regression analysis indicated a correlation between bimanual performance and wPLI value of $M1_L$–$M1_R$, we also examined the correlation between wPLI value of $M1_L$–$M1_R$ and PMd_R–$M1_L$ in each group separately and we found a significant correlation in older adults only ($r = 0.752$, $p = 5 \times 10^{-4}$).

4.6 | Correlation between structural (KA) and functional connectivity (wPLI)

Unlike the younger adults who did not show any significant correlation between KA and wPLI for the intra-hemispheric pathways, the older adults displayed significant correlations between wPLI in the left intra-hemispheric PMd-M1 connection and significant KA values for the $M1_L$–$M1_R$ and PMd_R–$M1_L$ connections; ($r = -0.574$ and
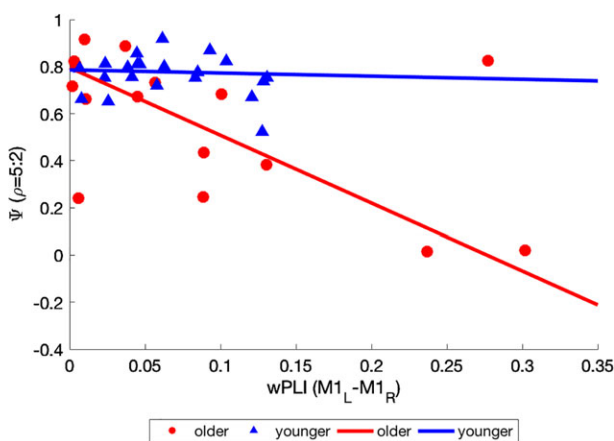
FIGURE 8 Scatter plots of bimanual performance (Ψ) versus wPLI and KA. Left panel: Increased structural connectivity between $PM1_R$–$M1_L$ was significantly associated with less coordinated bimanual performance in 1:1 ratio within the young group. Right panel: Increased functional coupling between $M1_L$–$M1_R$ was significantly associated with less coordinated bimanual performance in 5:2 ratio within the group of older adults [Color figure can be viewed at wileyonlinelibrary.com]
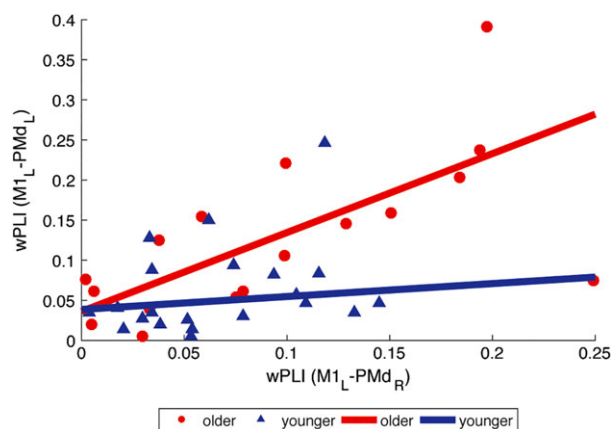
FIGURE 9 Scatter plot representing the significant relationship between intra-hemispheric and inter-hemispheric functional couplings. Only in older adults, greater wPLI value of PMd$_L$–M1$_L$ was associated with higher wPLI value of PMd$_R$–M1$_R$ [Color figure can be viewed at wileyonlinelibrary.com]

$p = 0.016$) and ($r = -0.502$ and $p = 0.04$), respectively (see Figure 10 and Table A12 in the Appendix for more details).

5 | DISCUSSION

We assessed age-related differences in the quality of bimanual motor performance, as well as structural and functional connectivity. To quantify this, we estimated the strength of frequency locking as a measure of bimanual coordination, the kurtosis anisotropy resulting from DWI tractography, and the phase synchronization of beta band activity of source reconstructed EEG activity during rest, respectively. We particularly focused on potential correlations between these measures within the context of the bimanual motor network.

We found wPLI values between PMd$_L$ and M1$_L$ to be correlated with the KA values of PMd$_R$–M1$_L$ but only in older adults. In addition, less coherent structural connectivity between PMd$_R$ and M1$_L$ was associated with better performance in the arguably simplest motor

subtask (1:1) in younger adults. In the older group, wPLI values between PMd$_L$ and M1$_L$ were also correlated with the KA values between M1$_L$ and M1$_R$. And, the phase synchronization between bilateral M1s (M1$_L$–M1$_R$) was associated with better motor performance in 5:2 ratio in older adults.

5.1 | Age-related differences in connectivity in relation with motor performance

KA values in all reconstructed fiber tracts were lower in older relative to younger adults. We consider this affirmative for the statement that white matter microstructural organization within the cortical motor network degenerates with advancing age. In fact, the results are in line with previous DWI studies (Abe et al., 2002; Coxon, Van Impe, Wenderoth, & Swinnen, 2012; Fujiyama, Van Soom, Rens, Gooijers, et al., 2016; Serbruyns et al., 2015; Sullivan et al., 2001), with the largest, significant decline in KA in the right intra-hemispheric PMd$_R$–M1$_R$ connection, as suggested by Ni et al. (2015). However, we cannot exclude that these results might have been influenced by partial volume effects due to the atrophy of white matter fibers in older subjects.

Consistent with resting state fMRI work by Solesio-Jofre et al. (2014), who reported age-related increase in functional connectivity within the bilateral motor network, we found increased wPLI values in older adults, particularly in the left intra-hemispheric pathway between PMd$_L$ and M1$_L$. Within the group of older adults, bimanual performance on the 5:2 ratio, in which the left hand rotates faster than the right hand, correlated negatively with the wPLI values of the M1$_L$–M1$_R$ connection, consistent with the fMRI results from Solesio-Jofre et al. (2014). They also found significant correlations between increased inter-hemispheric functional connectivity in motor regions at rest and reduced quality of motor performance. Our results thus indicate that an increased functional coupling between M1s is accompanied with less coordinated bimanual performance in older adults. In addition, within the group of younger adults, KA values between PMd$_R$ and M1$_L$ showed a significant negative correlation with bimanual performance.
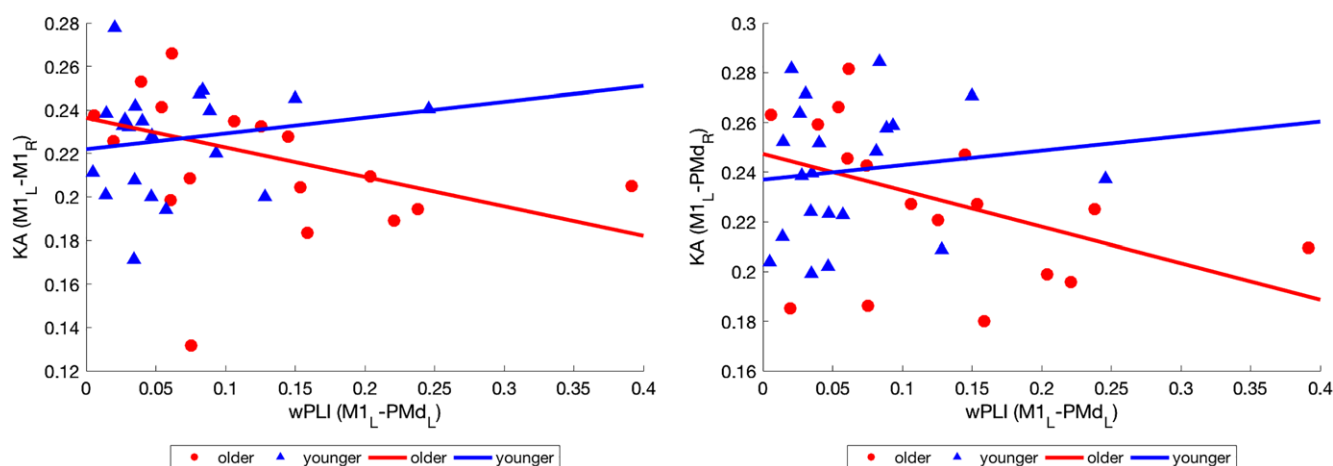

FIGURE 10 Scatter plots representing intra-hemispheric wPLI versus KA values. Left panel: Only in the older adults, larger wPLI values of PMd$_L$–M1$_L$ were associated with lower KA values of M1$_L$–M1$_R$ and PMd$_R$–M1$_L$ (right panel) [Color figure can be viewed at wileyonlinelibrary.com]

5.2 | Intra- and inter-hemispheric functional connectivity

The relationship between inter- and intra-hemispheric functional coupling during resting state was examined based on the model by Daffertshofer et al. (2005). Previous studies suggested that intra-cortical inhibition is related to shaping the output from M1s (Di Lazzaro et al., 1998; Donoghue, Hess, & Sanes, 1996). We did not find a significant correlation between intra- and inter-hemispheric functional coupling in the younger group, but the wPLI values of PMd_R–$M1_L$ in the older adults group correlated positively with wPLI values of PMd_L–$M1_L$ and $M1_L$–$M1_R$. This implies that differences in functional coupling between PMd_L and $M1_L$ are correlated with the functional coupling between PMd_R and $M1_L$. Hence, increased functional coupling between PMd_R and $M1_L$ in older adults may affect (increase) the functional coupling between M1s, which here negatively correlated with the quality of motor performance in the older group. Our results confirm the notion by Stinear and Byblow (2003) and Daffertshofer et al. (2005) that intra-hemispheric connectivity between PMd and M1 can be related to precise bimanual movement. Consequently, the left intra-hemispheric functional coupling may be responsible for reduced quality of bimanual motor performance in the elderly.

In more detail, we estimated Spearmen rank coefficients to test for correlations between wPLI values of five different pathways within the bimanual motor network. Only in older adults, the wPLI value between PMd_L–$M1_L$ correlated positively with the wPLI value of PMd_R–$M1_L$ connection. This is in line with (Fujiyama, Hinder, & Summers, 2013) and suggests left hemisphere (PMd_L) to be involved in inhibitory processing related to impulse control. Moreover, the significant correlation between PMd_L–$M1_L$ and PMd_R–$M1_L$ indicates the effect of both ipsilateral and contralateral PMd on $M1_L$ to control right hand movement only in older adults, which is in line with previous studies suggesting the involvement of both ipsilateral and contralateral PMd in the output from M1 in older adults (Fujiyama et al., 2013; Zimerman, Heise, Gerloff, Cohen, & Hummel, 2014).

5.3 | Structural versus functional connectivity

We investigated the relationship between intra-hemispheric KA values, derived from the deterministic white matter tractography, and wPLI values of all five pathways within each age group. Only in the group of older adults, lower KA values of inter-hemispheric tracts ($M1_L$–$M1_R$ and PMd_R–$M1_L$) were associated with higher wPLI values (higher functional coupling) of PMd_L–$M1_L$. This result supports the hypothesis that reduced microstructural white matter organization is related to a misbalance of functional coupling, in particular, left intra-hemispheric functional coupling between PMd_L–$M1_L$ is associated with age-related differences in inter-hemispheric structural connectivity of $M1_L$–$M1_R$ and PMd_R–$M1_L$.

The focus of the present study was to explore the relationships between functional connectivity inspired by the model by Daffertshofer et al. (2005) as a function of motor performance and, most importantly, the effect of structural organization of these tracts on the functional connectivity. Only in the older adult group, the left intra-hemispheric functional coupling correlated with functional coupling between PMd_R and $M1_L$. Only in the older adult group, the left intra-hemispheric neural synchronization correlated with inter-hemispheric structural connectivity.

The functional coupling between bilateral M1s in the older adults suggests its importance in properly performing the bimanual performance (5:2 ratio). In this group, the increased intra-hemispheric phase synchronization (PMd_L–$M1_L$) correlated with a decreased inter-hemispheric microstructural organization (PMd_R–$M1_L$ and $M1_L$–$M1_R$ tracts). Since phase synchronization of PMd_L–$M1_L$ also correlated with the phase synchronization between PMd_R and $M1_L$, any deficits in functional coupling between PMd_L and $M1_L$ appear to affect the inter-hemispheric functional coupling between PMd_R and $M1_L$, by this, the aforementioned $M1_L$–$M1_R$ coupling.

Taken together, the functional coupling in the left intra-hemispheric (PMd_L–$M1_L$) connection in older adults was associated with differences in both structural and functional connectivity between PMd_R and $M1_L$, which played an important role in the quality of bimanual performance in younger adults. This result is consistent with the findings by Fujiyama, Van Soom, Rens, Cuypers, et al. (2016) and Hinder et al. (2012) for the involvement of left PMd in bimanual performance.

5.4 | Limitations

The adopted DTI approach is widely used one for modeling of white matter microstructural organization, see, for example, Basser, Mattiello, and LeBihan (1994); Berman, Berger, Mukherjee, and Henry (2004), and Weiss et al. (2015) or more recent applications in the motor network (Ballester-Plane et al., 2017; Eixarch, Munoz-Moreno, Bargallo, Batalle, & Gratacos, 2016; Galantucci et al., 2017; Jarbo & Verstynen, 2015; Lee et al., 2017; Lee, Park, Park, & Hong, 2015; Misaghi, Zhang, Gracco, De Nil, & Beal, 2018). Unfortunately, as of yet there is no "gold standard" for DW-MRI based in vivo fiber tractography assessments (Farquharson et al., 2013; Jones, 2008; Tournier et al., 2011). Approaches can be deterministic, like the one used here, or probabilistic. Recently, however, Kupper et al. (2015), Khalsa, Mayhew, Chechlacz, Bagary, and Bagshaw (2014), Schlaier et al. (2017) and Sarwar, Ramamohanarao, and Zalesky (2018) showed that deterministic tractography often agrees with probabilistic tractography. While this may be considered convincing evidence, studies like (Jeurissen, Leemans, Jones, Tournier, & Sijbers, 2011) render the need for future studies to address this comparison in more detail.

6 | CONCLUSIONS

The significant correlation between intra- and inter-hemispheric neural phase synchronization in the aging brain appears to stem from reduced structural connectivity in inter-hemispheric fibers. Age-related differences in inter-hemispheric structural connectivity may hence be responsible for the deterioration of intra-hemispheric neural synchronization and its significant association to the inter-hemispheric neural phase synchronization. This may account for poor bimanual performance in older adults but further research is required to substantiate this observation.

ORCID

Parinaz Babaeeghazvini https://orcid.org/0000-0002-5640-6849
Laura Milena Rueda-Delgado https://orcid.org/0000-0002-8730-8977
Hamed Zivari Adab https://orcid.org/0000-0002-4971-2952
Stephan Swinnen https://orcid.org/0000-0001-7173-435X
Andreas Daffertshofer https://orcid.org/0000-0001-9107-3552

REFERENCES

Abe, O., Aoki, S., Hayashi, N., Yamada, H., Kunimatsu, A., Mori, H., … Ohtomo, K. (2002). Normal aging in the central nervous system: Quantitative MR diffusion-tensor analysis. *Neurobiology of Aging*, *23*, 433–441. https://doi.org/10.1016/S0197-4580(01)00318-9

Armatas, C. A., Summers, J. J., & Bradshaw, J. L. (1994). Mirror movements in normal adult subjects. *Journal of Clinical and Experimental Neuropsychology*, *16*, 405–413. https://doi.org/10.1080/01688639408402651

Ballester-Plane, J., Schmidt, R., Laporta-Hoyos, O., Junque, C., Vazquez, E., Delgado, I., … Pueyo, R. (2017). Whole-brain structural connectivity in dyskinetic cerebral palsy and its association with motor and cognitive function. *Human Brain Mapping*, *38*, 4594–4612. https://doi.org/10.1002/hbm.23686

Basser, P. J., Mattiello, J., & LeBihan, D. (1994). MR diffusion tensor spectroscopy and imaging. *Biophysical Journal*, *66*(1), 259–267. https://doi.org/10.1016/S0006-3495(94)80775-1

Basser, P. J., Pajevic, S., Pierpaoli, C., Duda, J., & Aldroubi, A. (2000). In vivo fiber tractography using DT-MRI data. *Magnetic Resonance in Medicine*, *44*, 625–632. https://doi.org/10.1002/1522-2594(200010)44:43.0.CO;2-O

Berman, J. I., Berger, M. S., Mukherjee, P., & Henry, R. G. (2004). Diffusion-tensor imaging-guided tracking of fibers of the pyramidal tract combined with intraoperative cortical stimulation mapping in patients with gliomas. *Journal of Neurosurgery*, *101*(1), 66–72. https://doi.org/10.3171/jns.2004.101.1.0066

Boussaoud, D., & Wise, S. P. (1993). Primate frontal cortex: Neuronal activity following attentional versus intentional cues. *Experimental Brain Research*, *95*, 15–27. https://doi.org/10.1007/BF00229650

Buchner, H., Knoll, G., Fuchs, M., Rienacker, A., Beckmann, R., Wagner, M., … Pesch, J. (1997). Inverse localization of electric dipole current sources in finite element models of the human head. *Electroencephalography and Clinical Neurophysiology*, *102*, 267–278. https://doi.org/10.1016/S0013-4694(96)95698-9

Chalavi, S., Zivari Adab, H., Pauwels, L., Beets, I. A., van Ruitenbeek, P., Boisgontier, M. P., … Swinnen, S. P. (2016). Anatomy of subcortical structures predicts age-related differences in skill acquisition. *Cerebral Cortex*, *28*, 459–473. https://doi.org/10.1093/cercor/bhw382

Coxon, J. P., Van Impe, A., Wenderoth, N., & Swinnen, S. P. (2012). Aging and inhibitory control of action: Cortico-subthalamic connection strength predicts stopping performance. *Journal of Neuroscience*, *32*, 8401–8412. https://doi.org/10.1523/JNEUROSCI.6360-11.2012

Crammond, D. J., & Kalaska, J. F. (1994). Modulation of preparatory neuronal activity in dorsal premotor cortex due to stimulus-response compatibility. *Journal of Neurophysiology*, *71*, 1281–1284. https://doi.org/10.1152/jn.1994.71.3.1281

Daffertshofer, A., Peper, C. E., & Beek, P. J. (2005). Stabilization of bimanual coordination due to active interhemispheric inhibition: A dynamical account. *Biological Cybernetics*, *92*, 101–109. https://doi.org/10.1007/s00422-004-0539-6

Daffertshofer, A., Peper, C. E., Frank, T. D., & Beek, P. J. (2000). Spatio-temporal patterns of encephalographic signals during polyrhythmic tapping. *Human Movement Science*, *19*, 475–498. https://doi.org/10.1016/S0167-9457(00)00032-4

Daffertshofer, A., van den Berg, C., & Beek, P. J. (1999). A dynamical model for mirror movements. *Physica D: Nonlinear Phenomena*, *132*, 243–266. https://doi.org/10.1016/S0167-2789(99)00044-5

Darvas, F., Pantazis, D., Kucukaltun-Yildirim, E., & Leahy, R. M. (2004). Mapping human brain function with MEG and EEG: Methods and validation. *NeuroImage*, *23*, 289–299. https://doi.org/10.1016/j.neuroimage.2004.07.014

Di Lazzaro, V., Restuccia, D., Oliviero, A., Profice, P., Ferrara, L., Insola, A., … Rothwell, J. C. (1998). Magnetic transcranial stimulation at intensities below active motor threshold activates intracortical inhibitory circuits. *Experimental Brain Research*, *119*, 265–268. https://doi.org/10.1007/s002210050341

Di Pellegrino, G., & Wise, S. P. (1993). Visuospatial versus visuomotor activity in the premotor and prefrontal cortex of a primate. *Journal of Neuroscience*, *13*, 1227–1243. https://doi.org/10.1523/JNEUROSCI.13-03-01227

Donoghue, J. P., Hess, G., & Sanes, J. N. (1996). Motor cortical substrates and mechanisms for learning. In J. R. Bloedel, T. J. Ebner, & S. P. Wise (Eds.), *Acquisition of motor behavior in vertebrates* (pp. 363–386). Cambridge, MA: MIT Press.

Eixarch, E., Munoz-Moreno, E., Bargallo, N., Batalle, D., & Gratacos, E. (2016). Motor and cortico-striatal-thalamic connectivity alterations in intrauterine growth restriction. *American Journal of Obstetrics and Gynecology*, *214*(725), e721–e729. https://doi.org/10.1016/j.ajog.2015.12.028

Farquharson, S., Tournier, J. D., Calamante, F., Fabinyi, G., Schneider-Kolsky, M., Jackson, G. D., & Connelly, A. (2013). White matter fiber tractography: Why we need to move beyond DTI. *Journal of Neurosurgery*, *118*(6), 1367–1377. https://doi.org/10.3171/2013.2.jns121294

Fujiyama, H., Hinder, M. R., & Summers, J. J. (2013). Functional role of left PMd and left M1 during preparation and execution of left hand movements in older adults. *Journal of Neurophysiology*, *110*, 1062–1069. https://doi.org/10.1152/jn.00075.2013

Fujiyama, H., Van Soom, J., Rens, G., Cuypers, K., Heise, K. F., Levin, O., & Swinnen, S. P. (2016). Performing two different actions simultaneously: The critical role of interhemispheric interactions during the preparation of bimanual movement. *Cortex*, *77*, 141–154. https://doi.org/10.1016/j.cortex.2016.02.007

Fujiyama, H., Van Soom, J., Rens, G., Gooijers, J., Leunissen, I., Levin, O., & Swinnen, S. P. (2016). Age-related changes in frontal network structural and functional connectivity in relation to bimanual movement control. *Journal of Neuroscience*, *36*, 1808–1822. https://doi.org/10.1523/JNEUROSCI.3355-15.2016

Galantucci, S., Agosta, F., Stefanova, E., Basaia, S., van den Heuvel, M. P., Stojkovic, T., … Filippi, M. (2017). Structural brain connectome and cognitive impairment in parkinson disease. *Radiology*, *283*, 515–525. https://doi.org/10.1148/radiol.2016160274

Gerloff, C., Corwell, B., Chen, R., Hallett, M., & Cohen, L. G. (1998). The role of the human motor cortex in the control of complex and simple finger movement sequences. *Brain*, *121*, 1695–1709. https://doi.org/10.1093/brain/121.9.1695

Goble, D. J., Coxon, J. P., Van Impe, A., De Vos, J., Wenderoth, N., & Swinnen, S. P. (2010). The neural control of bimanual movements in the elderly: Brain regions exhibiting age-related increases in activity, frequency-induced neural modulation, and task-specific compensatory recruitment. *Human Brain Mapping*, *31*, 1281–1295. https://doi.org/10.1002/hbm.20943

Gooijers, J., Caeyenberghs, K., Sisti, H. M., Geurts, M., Heitger, M. H., Leemans, A., & Swinnen, S. P. (2013). Diffusion tensor imaging metrics of the corpus callosum in relation to bimanual coordination: Effect of task complexity and sensory feedback. *Human Brain Mapping*, *34*, 241–252. https://doi.org/10.1002/hbm.21429

Hardmeier, M., Hatz, F., Bousleiman, H., Schindler, C., Stam, C. J., & Fuhr, P. (2014). Reproducibility of functional connectivity and graph measures based on the phase lag index (PLI) and weighted phase lag index (wPLI) derived from high resolution EEG. *PLoS One*, *9*(10), e108648. https://doi.org/10.1371/journal.pone.0108648

Heuninckx, S., Wenderoth, N., Debaere, F., Peeters, R., & Swinnen, S. P. (2005). Neural basis of aging: The penetration of cognition into action

control. *The Journal of Neuroscience, 25,* 6787–6796. https://doi.org/10.1523/jneurosci.1263-05.2005

Heuninckx, S., Wenderoth, N., & Swinnen, S. P. (2008). Systems neuroplasticity in the aging brain: Recruiting additional neural resources for successful motor performance in elderly persons. *The Journal of Neuroscience, 28,* 91–99. https://doi.org/10.1523/JNEUROSCI.3300-07.2008

Hinder, M. R., Fujiyama, H., & Summers, J. J. (2012). Premotor-motor interhemispheric inhibition is released during movement initiation in older but not young adults. *PLoS One, 7,* e52573. https://doi.org/10.1371/journal.pone.0052573

Holdefer, R. N., Sadleir, R., & Russell, M. J. (2006). Predicted current densities in the brain during transcranial electrical stimulation. *Clinical Neurophysiology, 117,* 1388–1397. https://doi.org/10.1016/j.clinph.2006.02.020

Houweling, S., Beek, P. J., & Daffertshofer, A. (2010). Spectral changes of interhemispheric crosstalk during movement instabilities. *Cerebral Cortex, 20,* 2605–2013. https://doi.org/10.1093/cercor/bhq008

Iacono, M. I., Neufeld, E., Akinnagbe, E., Bower, K., Wolf, J., Vogiatzis Oikonomidis, I., … Angelone, L. M. (2015). MIDA: A multimodal imaging-based detailed anatomical model of the human head and neck. *PLoS One, 10,* e0124126. https://doi.org/10.1371/journal.pone.0124126

Irfanoglu, M. O., Walker, L., Sarlls, J., Marenco, S., & Pierpaoli, C. (2012). Effects of image distortions originating from susceptibility variations and concomitant fields on diffusion MRI tractography results. *NeuroImage, 61,* 275–288. https://doi.org/10.1016/j.neuroimage.2012.02.054

Jarbo, K., & Verstynen, T. D. (2015). Converging structural and functional connectivity of orbitofrontal, dorsolateral prefrontal, and posterior parietal cortex in the human striatum. *Journal of Neuroscience, 35,* 3865–3878. https://doi.org/10.1523/JNEUROSCI.2636-14.2015

Jeurissen, B., Leemans, A., Jones, D. K., Tournier, J.-D., & Sijbers, J. (2011). Probabilistic fiber tracking using the residual bootstrap with constrained spherical deconvolution. *Human Brain Mapping, 32*(3), 461–479. https://doi.org/10.1002/hbm.21032

Jones, D. K. (2008). Studying connections in the living human brain with diffusion MRI. *Cortex, 44,* 936–952. https://doi.org/10.1016/j.cortex.2008.05.002

Khalsa, S., Mayhew, S. D., Chechlacz, M., Bagary, M., & Bagshaw, A. P. (2014). The structural and functional connectivity of the posterior cingulate cortex: Comparison between deterministic and probabilistic tractography for the investigation of structure–function relationships. *NeuroImage, 102,* 118–127. https://doi.org/10.1016/j.neuroimage.2013.12.022

Kupper, H., Groeschel, S., Alber, M., Klose, U., Schuhmann, M. U., & Wilke, M. (2015). Comparison of different tractography algorithms and validation by intraoperative stimulation in a child with a brain tumor. *Neuropediatrics, 46*(1), 72–75. https://doi.org/10.1055/s-0034-1395346

Lee, D., Pae, C., Lee, J. D., Park, E. S., Cho, S. R., Um, M. H., … Park, H. J. (2017). Analysis of structure-function network decoupling in the brain systems of spastic diplegic cerebral palsy. *Human Brain Mapping, 38,* 5292–5306. https://doi.org/10.1002/hbm.23738

Lee, D. H., Park, J. W., Park, S. H., & Hong, C. (2015). Have you ever seen the impact of crossing fiber in DTI?: Demonstration of the corticospinal tract pathway. *PLoS One, 10*(7), e0112045.

Leemans, A., Jeurissen, B., Sijbers, J., & Jones, D. K. (2009). *ExploreDTI: a graphical toolbox for processing, analyzing, and visualizing diffusion MR data.* Paper presented at the ISMRM, 17th Scientific Meeting and Exhibition, Hawaii.

Leemans, A., Sijbers, J., De Backer, S., Vandervliet, E., & Parizel, P. M. (2005). Affine coregistration of diffusion tensor magnetic resonance images using mutual information. *Advanced Concepts for Intelligent Vision Systems in Proc, 3708,* 523–530. https://doi.org/10.1007/11558484_66

Leinsinger, G. L., Heiss, D. T., Jassoy, A. G., Pfluger, T., Hahn, K., & Danek, A. (1997). Persistent mirror movements: Functional MR imaging of the hand motor cortex. *Radiology, 203,* 545–552. https://doi.org/10.1148/radiology.203.2.9114119

Mayka, M. A., Corcos, D. M., Leurgans, S. E., & Vaillancourt, D. E. (2006). Three-dimensional locations and boundaries of motor and premotor cortices as defined by functional brain imaging: A meta-analysis. *NeuroImage, 31,* 1453–1474. https://doi.org/10.1016/j.neuroimage.2006.02.004

Misaghi, E., Zhang, Z., Gracco, V. L., De Nil, L. F., & Beal, D. S. (2018). White matter tractography of the neural network for speech-motor control in children who stutter. *Neuroscience Letters, 668,* 37–42. https://doi.org/10.1016/j.neulet.2018.01.009

Nasreddine, Z. S., Phillips, N. A., Bedirian, V., Charbonneau, S., Whitehead, V., Collin, I., … Chertkow, H. (2005). The Montreal cognitive assessment, MoCA: A brief screening tool for mild cognitive impairment. *Journal of the American Geriatrics Society, 53,* 695–699. https://doi.org/10.1111/j.1532-5415.2005.53221.x

Ni, Z., Isayama, R., Castillo, G., Gunraj, C., Saha, U., & Chen, R. (2015). Reduced dorsal premotor cortex and primary motor cortex connectivity in older adults. *Neurobiology of Aging, 36,* 301–303. https://doi.org/10.1016/j.neurobiolaging.2014.08.017

Nolan, H., Whelan, R., & Reilly, R. B. (2010). FASTER: Fully automated statistical Thresholding for EEG artifact rejection. *Journal of Neuroscience Methods, 192,* 152–162. https://doi.org/10.1016/j.jneumeth.2010.07.015

Nolte, G., Bai, O., Wheaton, L., Mari, Z., Vorbach, S., & Hallett, M. (2004). Identifying true brain interaction from EEG data using the imaginary part of coherence. *Clinical Neurophysiology, 15,* 2292–2307. https://doi.org/10.1016/j.clinph.2004.04.029

Nusbaum, A. O., Tang, C. Y., Buchsbaum, M. S., Wei, T. C., & Atlas, S. W. (2001). Regional and global changes in cerebral diffusion with normal aging. *American Journal of Neuroradiology, 22,* 136–142.

O'Sullivan, M., Morris, R. G., Huckstep, B., Jones, D. K., Williams, S. C., & Markus, H. S. (2004). Diffusion tensor MRI correlates with executive dysfunction in patients with ischaemic leukoaraiosis. *Journal of Neurology, Neurosurgery, and Psychiatry, 75*(3), 441–447. https://doi.org/10.1136/jnnp.2003.014910

Oldfield, R. C. (1971). The assessment and analysis of handedness: The Edinburgh inventory. *Neuropsychologia, 9,* 97–113. https://doi.org/10.1016/0028-3932(71)90067-4

Oostenveld, R., Fries, P., Maris, E., & Schoffelen, J. M. (2011). FieldTrip: Open source software for advanced analysis of MEG, EEG, and invasive electrophysiological data. *Computational Intelligence and Neuroscience, 2011,* 1–9. https://doi.org/10.1155/2011/156869

Pinheiro, J., & Bates, D. (2000). *Mixed-effects models in S and S-PLUS* (1st ed.). New York, NY: Springer-Verlag.

Poot, D. H., den Dekker, A. J., Achten, E., Verhoye, M., & Sijbers, J. (2010). Optimal experimental design for diffusion kurtosis imaging. *IEEE Transactions on Medical Imaging, 29,* 819–829. https://doi.org/10.1109/TMI.2009.2037915

Rueda-Delgado, L. M., Solesio-Jofre, E., Mantini, D., Dupont, P., Daffertshofer, A., & Swinnen, S. P. (2017). Coordinative task difficulty and behavioural errors are associated with increased long-range beta band synchronization. *NeuroImage, 146,* 883–893. https://doi.org/10.1016/j.neuroimage.2016.10.030

Sarwar, T., Ramamohanarao, K., & Zalesky, A. (2018). Mapping connectomes with diffusion MRI: Deterministic or probabilistic tractography? *Magnetic Resonance in Medicine,* 1–17 (in press). https://doi.org/10.1002/mrm.27471

Schlaier, J. R., Beer, A. L., Faltermeier, R., Fellner, C., Steib, K., Lange, M., … Anthofer, J. M. (2017). Probabilistic vs. deterministic fiber tracking and the influence of different seed regions to delineate cerebellar-thalamic fibers in deep brain stimulation. *European Journal of Neuroscience, 45,* 1623–1633. https://doi.org/10.1111/ejn.13575

Serbruyns, L., Gooijers, J., Caeyenberghs, K., Meesen, R. L., Cuypers, K., Sisti, H. M., … Swinnen, S. P. (2015). Bimanual motor deficits in older adults predicted by diffusion tensor imaging metrics of corpus callosum subregions. *Brain Structure and Function, 220,* 273–290. https://doi.org/10.1007/s00429-013-0654-z

Shen, L., & Alexander, G. E. (1997). Neural correlates of a spatial sensory-to-motor transformation in primary motor cortex. *Journal of Neurophysiology, 77,* 1171–1194. https://doi.org/10.1152/jn.1997.77.3.1171

Sisti, H. M., Geurts, M., Clerckx, R., Gooijers, J., Coxon, J. P., Heitger, M. H., … Swinnen, S. P. (2011). Testing multiple coordination constraints with a novel bimanual visuomotor task. *PLoS One, 6*(8), e23619. https://doi.org/10.1371/journal.pone.0023619

Solesio-Jofre, E., Serbruyns, L., Woolley, D. G., Mantini, D., Beets, I. A., & Swinnen, S. P. (2014). Aging effects on the resting state motor network and interlimb coordination. *Human Brain Mapping, 35,* 3945–3961. https://doi.org/10.1002/hbm.22450

Stam, C. J., Nolte, G., & Daffertshofer, A. (2007). Phase lag index: Assessment of functional connectivity from multi channel EEG and MEG with diminished bias from common sources. *Human Brain Mapping, 28,* 1178–1193. https://doi.org/10.1002/hbm.20346

Stinear, C. M., & Byblow, W. D. (2003). Role of intracortical inhibition in selective hand muscle activation. *Journal of Neurophysiology*, 89, 2014–2020. https://doi.org/10.1152/jn.00925.2002

Stinear, J. W., & Byblow, W. D. (2002). Disinhibition in the human motor cortex is enhanced by synchronous upper limb movements. *Journal of Physiology*, 543, 307–316. https://doi.org/10.1113/jphysiol.2002.023986

Sullivan, E. V., Adalsteinsson, E., Hedehus, M., Ju, C., Moseley, M., Lim, K. O., & Pfefferbaum, A. (2001). Equivalent disruption of regional white matter microstructure in ageing healthy men and women. *Neuroreport*, 12, 99–104. https://doi.org/10.1097/00001756-200101220-00027

Tax, C. M., Otte, W. M., Viergever, M. A., Dijkhuizen, R. M., & Leemans, A. (2015). REKINDLE: Robust extraction of kurtosis INDices with linear estimation. *Magnetic Resonance in Medicine*, 73, 794–808. https://doi.org/10.1002/mrm.25165

Tournier, J. D., Mori, S., & Leemans, A. (2011). Diffusion tensor imaging and beyond. *Magnetic Resonance in Medicine*, 65, 1532–1556. https://doi.org/10.1002/mrm.22924

Van Hecke, W., Leemans, A., D'Agostino, E., De Backer, S., Vandervliet, E., Parizel, P. M., & Sijbers, J. (2007). Nonrigid coregistration of diffusion tensor images using a viscous fluid model and mutual information. *IEEE Transactions on Medical Imaging*, 26, 1598–1612. https://doi.org/10.1109/TMI.2007.906786

Van Veen, B. D., van Drongelen, W., Yuchtman, M., & Suzuki, A. (1997). Localization of brain electrical activity via linearly constrained minimum variance spatial filtering. *IEEE Transactions on Biomedical Engineering*, 44, 867–880. https://doi.org/10.1109/10.623056

Vinck, M., Oostenveld, R., van Wingerden, M., Battaglia, F., & Pennartz, C. M. (2011). An improved index of phase-synchronization for electrophysiological data in the presence of volume-conduction, noise and sample-size bias. *NeuroImage*, 55, 1548–1565. https://doi.org/10.1016/j.neuroimage.2011.01.055

Wagner, S., Rampersad, S. M., Aydin, U., Vorwerk, J., Oostendorp, T. F., Neuling, T., ... Wolters, C. H. (2014). Investigation of tDCS volume conduction effects in a highly realistic head model. *Journal of Neural Engineering*, 11, 016002. https://doi.org/10.1088/1741-2560/11/1/016002

Wahl, M., Lauterbach-Soon, B., Hattingen, E., Jung, P., Singer, O., Volz, S., ... Ziemann, U. (2007). Human motor corpus callosum: Topography, somatotopy, and link between microstructure and function. *The Journal

of Neuroscience*, 27, 12132–12138. https://doi.org/10.1523/JNEUROSCI.2320-07.2007

Weiss, C., Tursunova, I., Neuschmelting, V., Lockau, H., Nettekoven, C., Oros-Peusquens, A. M., ... Grefkes, C. (2015). Improved nTMS- and DTI-derived CST tractography through anatomical ROI seeding on anterior pontine level compared to internal capsule. *NeuroImage: Clinical*, 7, 424–437.

Wise, S. P., Di Pellegrino, G., & Boussaoud, D. (1992). Primate premotor cortex: Dissociation of visuomotor from sensory signals. *Journal of Neurophysiology*, 68, 969–972. https://doi.org/10.1152/jn.1992.68.3.969

Wolters, C. H., Anwander, A., Tricoche, X., Weinstein, D., Koch, M. A., & MacLeod, R. S. (2006). Influence of tissue conductivity anisotropy on EEG/MEG field and return current computation in a realistic head model: A simulation and visualization study using high-resolution finite element modeling. *NeuroImage*, 30, 813–826. https://doi.org/10.1016/j.neuroimage.2005.10.014

Zimerman, M., Heise, K. F., Gerloff, C., Cohen, L. G., & Hummel, F. C. (2014). Disrupting the ipsilateral motor cortex interferes with training of a complex motor task in older adults. *Cerebral Cortex*, 24, 1030–1036. https://doi.org/10.1093/cercor/bhs385

Zivari Adab, H., Chalavi, S., Beets, I. A. M., Gooijers, J., Leunissen, I., Cheval, B., ... Boisgontier, M. P. (2018). White matter microstructural organization of interhemispheric pathways predicts different stages of bimanual coordination learning in young and older adults. *European Journal of Neuroscience*, 47, 446–459. https://doi.org/10.1111/ejn.13841

APPENDIX: Details of the LME estimates and the Mann–Whitney tests

TABLE A1 LME estimates of fixed effects for the Ψ value

	Estimate	SE	t(df)	p-value
Intercept	**0.9190**	0.0379	24.281(88.502)	**<6.7 × 10⁻¹⁴**
Older vs. mean	−0.0358	0.0566	−0.632(88.502)	0.529
(5:2) vs. mean	**−0.1556**	0.0422	−3.690(76)	**<4.2 × 10⁻⁴**
(2:5) vs. mean	**−0.1652**	0.0422	−3.917(76)	**<1.9 × 10⁻⁴**
Older * (5:2) vs. mean	**−0.1706**	0.0630	−2.706(76)	**0.008**
Older * (2:5) vs. mean	**−0.1859**	0.0630	−2.949(76)	**0.004**

SE = standard error. Bold value represents the *p*-value which was lower than .05 (i.e., significance threshold α=0.05).

TABLE A2 LME estimates of random effects for the Ψ value

	Name	Variance	SE
Participant	Intercept	0.0114	0.0042
Residual		0.0187	0.00303

SE = standard error.

TABLE A3 *p*-values of the Mann–Whitney test of the Ψ values between two groups

Frequency ratio 1:1	0.091
Frequency ratio 2:5	**0.021**
Frequency ratio 5:2	**0.044**

Bold value represents the *p*-value which was lower than .05 (i.e., significance threshold α=0.05).

TABLE A4 LME estimates of fixed effects for the **KA** value

	Estimate	SE	t(df)	p-value
Intercept	**0.1912**	0.0066	29.165(101.341)	**<4.2 × 10⁻⁵¹**
Older vs. mean	−0.0074	0.0098	−0.759(101.341)	0.449
(M1$_L$–M1$_R$) vs. mean	**0.0349**	0.0068	5.161(152)	**<7.6 × 10⁻⁷**
(PMd$_L$–M1$_R$) vs. mean	**0.0534**	0.0068	7.889(152)	**<5.6 × 10⁻¹³**
(PMd$_R$–M1$_L$) vs. mean	**0.0494**	0.0068	7.309(152)	**<1.4 × 10⁻¹¹**
(PMd$_R$–M1$_R$) vs. mean	0.0030	0.0068	0.446(152)	0.656
Older * (M1$_L$–M1$_R$) vs. mean	−0.0044	0.0101	−0.432(152)	0.666
Older * (PMd$_L$–M1$_R$) vs. mean	**−0.0238**	0.0101	−2.355(152)	**0.020**
Older * (PMd$_R$–M1$_L$) vs. mean	−0.0061	0.0101	−0.601(152)	0.549
Older * (PMd$_R$–M1$_R$) vs. mean	−0.0105	0.0101	−1.040(152)	0.300

SE = standard error. Bold value represents the p-value which was lower than .05 (i.e., significance threshold α=0.05).

TABLE A5 LME estimates of random effects for the **KA** value

	Name	Variance	SE
Participant	Intercept	0.000422	0.000119
Residual		0.000480	0.000055

SE = standard error.

TABLE A6 p-values of the Mann–Whitney test of **KA**, **FA**, **MD**, **RD**, and **AD** values between two groups

	IQR_L KA	Median FA	Median MD	Median RD	Median AD
PMd$_R$–M1$_R$	**0.009**	**0.006**	**0.007**	**4.03 × 10⁻⁴**	0.490
PMd$_L$–M1$_L$	0.189	0.472	**0.005**	**0.008**	**0.043**
PMd$_R$–M1$_L$	0.199	0.340	0.060	**0.024**	0.758
PMd$_L$–M1$_R$	0.101	0.340	0.134	0.134	0.436
M1$_L$–M1$_R$	0.209	0.097	**0.046**	**0.007**	0.370

Bold value represents the p-value which was lower than .05 (i.e., significance threshold α=0.05).

TABLE A7 LME estimates of fixed effects for the **wPLI** value

	Estimate	SE	t(df)	p-value
Intercept	**0.0758**	0.0144	5.252(157.1)	**<4.8 × 10⁻⁷**
Older vs. mean	0.0633	0.0216	0.301(157.1)	0.764
(M1$_L$–M1$_R$) vs. mean	−0.0111	0.0179	−0.620(152)	0.536
(PMd$_L$–M1$_R$) vs. mean	−0.0244	0.0179	−1.364(152)	0.175
(PMd$_R$–M1$_L$) vs. mean	−0.0089	0.0179	−0.498(152)	0.619
(PMd$_L$–M1$_L$) vs. mean	−0.0135	0.0179	−0.755(152)	0.451
Older * (M1$_L$–M1$_R$) vs. mean	0.0113	0.0268	0.422(152)	0.674
Older * (PMd$_L$–M1$_R$) vs. mean	0.0250	0.0268	0.933(152)	0.352
Older * (PMd$_R$–M1$_L$) vs. mean	0.0224	0.0268	0.835(152)	0.405
Older * (PMd$_L$–M1$_L$) vs. mean	**0.0568**	0.0268	2.121(152)	**0.036**

SE = standard error. Bold value represents the p-value which was lower than .05 (i.e., significance threshold α=0.05).

TABLE A8 LME estimates of random effects for the **wPLI** value

	Name	Variance	SE
Participant	Intercept	0.001	0.00039
Residual		0.0034	0.00038

SE = standard error.

TABLE A9 *p*-values of the Mann–Whitney test of **wPLI** values between two groups

PMd_R–$M1_R$	0.758
PMd_L–$M1_L$	**0.018**
PMd_L–$M1_R$	0.490
PMd_R–$M1_L$	0.403
$M1_L$–$M1_R$	0.509

TABLE A10 Linear regression model predicting Ψ from **KA** and **wPLI**

Participants	Younger group		Older group	
Task	1:1 ratio		5:2 ratio	
Adjusted R^2	0.175		0.241	
Regression coefficient and *p*-value	*β*	*p*	*β*	*p*
(KA) PMd_R–$M1_R$	−0.004	0.986	0.073	0.758
(KA) PMd_L–$M1_L$	0.195	0.403	0.051	0.834
(KA) PMd_R–$M1_L$	**−0.552**	**0.012**	−0.067	0.777
(KA) PMd_L–$M1_R$	−0.124	0.710	−0.233	0.326
(KA) $M1_L$–$M1_R$	0.101	0.750	−0.162	0.493
(wPLI) PMd_R–$M1_R$	0.042	0.840	0.076	0.752
(wPLI) PMd_L–$M1_L$	0.072	0.730	−0.243	0.371
(wPLI) PMd_L–$M1_R$	0.185	0.363	0.403	0.076
(wPLI) PMd_R–$M1_L$	0.027	0.896	0.141	0.713
(wPLI) $M1_L$–$M1_R$	−0.185	0.369	**−0.540**	**0.031**

Bold value represents the *p*-value which was lower than .05 (i.e., significance threshold α=0.05).

TABLE A11 Spearman correlations between **wPLI** values in both groups

	Older group						Younger group					
	PMd_L–$M1_R$		$M1_L$–$M1_R$		PMd_R–$M1_L$		PMd_L–$M1_R$		$M1_L$–$M1_R$		PMd_R–$M1_L$	
	r	p	r	p	r	p	r	p	r	p	r	p
PMd_R–$M1_R$	0.042	0.874	0.223	0.390	0.150	0.567	0.209	0.363	−0.192	0.404	0.187	0.417
PMd_L–$M1_L$	0.113	0.667	0.461	0.063	**0.691**	**0.002**	−0.108	0.642	−0.213	0.354	0.361	0.108

Bold value represents the *p*-value which was lower than .05 (i.e., significance threshold α=0.05).

TABLE A12 Spearman correlations between **KA** and **wPLI** values in both groups

	Older group		Younger group	
	(wPLI) $M1_L$–PMd_L		(wPLI) $M1_L$–PMd_L	
	r	p	r	p
(KA) PMd_R–$M1_R$	−0.453	0.068	0.091	0.695
(KA) PMd_L–$M1_L$	−0.348	0.171	0.139	0.548
(KA) PMd_R–$M1_L$	**−0.502**	**0.040**	0.105	0.650
(KA) PMd_L–$M1_R$	−0.287	0.264	0.099	0.670
(KA) $M1_L$–$M1_R$	**−0.574**	**0.016**	0.164	0.478

Bold value represents the *p*-value which was lower than .05 (i.e., significance threshold α=0.05).